ship of the lateral prefrontal cortex relative to the temporal poles appear derived. Following Connolly (23), we decline to identify rami that border the human pars triangularis (part of Broca's area) on the left, although the general morphology in this region would be consistent with their existence. On the left (and to a lesser extent the right), a distinct Sylvian notch separates the temporal from the frontal lobe and continues caudally as a depression. This region corresponds to a Sylvian crest within the skull of LB1 that, in humans, sometimes occurs in particularly thick skulls and is correlated with Sylvian depressions on endocasts, although the brains are, if anything, more opercularized in the corresponding area (23).

The depression for the superior sagittal sinus on LB1's frontal lobes is bordered laterally by large convolutions [which probably contained additional furrows not reproduced on the endocast (23)] that curve around the rostral tip of the endocast onto the orbital surface and meet at the foramen caecum. Dimples separate these convolutions laterally from swellings that square off the frontal lobes and give their outline a ruffled appearance in dorsal view (Fig. 1A). Although hints of such contours may be seen in chimpanzee and hominin endocasts such as in the no. 2 specimen from Sterkfontein (9), the extent of these expansions in the frontal polar region of LB1 is unusual. This part of the prefrontal cortex in humans and apes consists of Brodmann's area 10, which in humans may be involved in higher cognitive processes such as the undertaking of initiatives and the planning of future activities (25). Human frontal lobes are not larger than expected for apes of similar brain volume (26), but area 10 is both absolutely and relatively enlarged in H. sapiens as compared with apes (25). LB1's polar convolutions appear derived compared with those of H. erectus and other early hominins. Unlike the frontal lobes, human temporal lobes appear to be somewhat larger than expected for an ape brain of human size (26–28); thus, LB1's extremely wide temporal lobes (brachycephaly; fig. S3) may represent another derived feature.

Our data show that LB1's well-convoluted brain could not have been a miniaturized version of the brain of either H. sapiens or H. erectus. Nevertheless, its similarities with H. erectus strongly suggest a phylogenetic connection, although its australopithecine-like brain/body size ratio and morphology of the femur and pelvis (29) are not expected in a miniaturized descendant of a larger-bodied H. erectus (which, instead, would be expected to scale allometrically along the ontogenetic curve predicted for H. erectus) (fig. S1). Although it is possible that H. floresiensis represented an endemic island dwarf that, over time, became subject to unusual allometric constraints, an

alternative hypothesis is that H. erectus and H. floresiensis may have shared a common ancestor that was an unknown small-bodied and small-brained hominin (1).

References and Notes

1. P. Brown et al., Nature 431, 1055 (2004).
2. R. L. Holloway, D. C. Broadfield, M. S. Yuan, The Human Fossil Record, Volume Three, Brain Endocasts–The Paleoneurological Evidence (Wiley-Liss, Hoboken, NJ, 2004).
3. M. J. Morwood et al., Nature 431, 1087 (2004).
4. M. Henneberg, A. Thorne, Before Farming (online journal) 4, article 2 (2004).
5. G. C. Conroy, M. W. Vannier, in Hominid Evolution: Past, Present and Future, P. V. Tobias, Ed. (Liss, New York, 1985), pp. 419–426.
6. G. C. Conroy, M. Vannier, P. V. Tobias, Science 247, 838 (1990).
7. G. C. Conroy et al., Science 280, 1730 (1998).
8. F. Spoor, N. Jeffery, F. Zonneveld, J. Anat. 197, 61 (2000).
9. Falk et al., J. Hum. Evol. 38, 695 (2000).
10. The CT-estimated cranial capacity was 417 cm³, as opposed to 380 cm³ measured with mustard seeds (1). The 37-cm³ difference is attributable to variation in how cranial holes were plugged and thus to measurement error associated with the current reconstructions.
11. A. Verloes, Orphanet Encyclopedia, www.orpha.net/data/patho/GB/uk-MVMSG.pdf (February 2004).
12. A. Kumar et al., J. Biosci. 27, 629 (2002).
13. W. H. Flower, J. Anthropol. Inst. G. B. Ireland 18, 3 (1889).
14. L. L. Cavalli-Sforza, in African Pygmies, L. L. Cavalli-Sforza, Ed. (Academic Press, New York, 1986), pp. 81–93.
15. B. T. Shea, R. C. Bailey, Am. J. Phys. Anthropol. 100, 311 (1996).
16. R. Passingham, New Scientist 27, 510 (1975).
17. A. H. Schultz, Primatologica I, 887 (1956).
18. H. Jerison, Evolution of the Brain and Intelligence (Academic Press, New York, 1973).
19. J. Diamond, Science 306, 2047 (2004).
20. M. LeMay, Am. J. Neuroradiol. 13, 493 (1992).
21. D. Falk, Am. J. Phys. Anthropol. 92, 81 (1993).
22. F. Weidenreich, Palaeontol. Sinica New Ser. D. 3, 1 (1938).
23. C. J. Connolly, External Morphology of the Primate Brain (Thomas, Springfield, IL, 1950).
24. D. Falk, Science 221, 1072 (1983).
25. K. Semendeferi et al., Am. J. Phys. Anthropol. 114, 224 (2001).
26. K. Semendeferi, in Evolutionary Anatomy of the Primate Cerebral Cortex, D. Falk, K. R. Gibson, Eds. (Cambridge Univ. Press, Cambridge, 2001), pp. 257–289.
27. K. Semendeferi, H. Damasio, J. Hum. Evol. 38, 317 (2000).
28. J. K. Rilling, R. A. Seligman, J. Hum. Evol. 42, 505 (2002).
29. C. Groves, Before Farming (online journal) 4, article 1 (2004).
30. We thank the National Geographic Society (grant 7760-04) and D. Hamlin for helping to bring this research to fruition. X. Wu of the Institute of Vertebrate Paleontology and Paleoanthropology, Chinese Academy of Sciences, provided the measurements for H. sapiens in Table 1; K. Mowbray of the American Museum of Natural History provided the cast of the microcephalic skull and pygmy skull; and B. Latimer and L. Jellema of the Cleveland Museum of Natural History loaned additional skeletal material. We appreciate T. Gebke and C. Tinscher's technical assistance in CT scanning, B. Macy's production of physical endocasts, B. Worthington's illustrations of LB1's endocast (Fig. 3), and E. Chambless's help with manuscript preparation.

Vasopressin and Oxytocin Excite Distinct Neuronal Populations in the Central Amygdala

Daniel Huber,[1] Pierre Veinante,[2] Ron Stoop[1]*

Vasopressin and oxytocin strongly modulate autonomic fear responses, through mechanisms that are still unclear. We describe how these neuropeptides excite distinct neuronal populations in the central amygdala, which provides the major output of the amygdaloid complex to the autonomic nervous system. We identified these two neuronal populations as part of an inhibitory network, through which vasopressin and oxytocin modulate the integration of excitatory information from the basolateral amygdala and cerebral cortex in opposite manners. Through this network, the expression and endogenous activation of vasopressin and oxytocin receptors may regulate the autonomic expression of fear.

The amygdala plays an important role in anxiety and fear behavior. Fear learning involves its lateral and basolateral parts, where

[1]Department of Cellular Biology and Morphology and Centre for Psychiatric Neuroscience, Department of Psychiatry, Centre Hospitalier Universitaire Vaudois, University of Lausanne, Switzerland. [2]Neurophysiologie Cellulaire et Intégrée, Unité Mixte de Recherche 7519, CNRS, Université Louis Pasteur, Strasbourg, France.

*To whom correspondence should be addressed. E-mail: rstoop@unil.ch

the association between incoming fearful and neutral stimuli leads to potentiation of synaptic transmission. These parts project to the central amygdala (CeA), whose efferents to the hypothalamus and brainstem trigger the autonomic expression of fear (1). Selective gating of synaptic transmission through the CeA could therefore modulate the fear response (2, 3). Indeed, recent studies suggest that increased inhibition within the CeA could underlie the anxiolytic effects of benzodiaze-

pines and alcohol (4, 5) and may also play a role in the extinction of conditioned fear through cortical afferents (6, 7).

The CeA expresses numerous neuropeptides and neuropeptide receptors, including high levels of receptors for vasopressin and oxytocin (8, 9). Activation of vasopressin and oxytocin receptors oppositely affects fear and anxiety-related behaviors. Vasopressin enhances aggressiveness, anxiety, and stress levels and the consolidation of fear memory (10–13). Oxytocin decreases anxiety and stress and facilitates social encounters, maternal care, and the extinction of conditioned avoidance behavior (13–17). At the cellular level, however, both neuropeptides increase neuronal excitability in various brain regions, including the CeA (18–20), which raises the question of whether a local neuronal network could underlie their opposite behavioral effects.

We first determined the distribution of vasopressin and oxytocin receptors in the CeA using autoradiography on horizontal rat brain sections (21). Binding of ^{125}I-labeled ligands revealed that expression of oxytocin receptors was restricted to the lateral and capsular division of the CeA (CeL/C) and vasopressin receptors in the medial part (CeM) (Fig. 1A). To determine the physiological effects of activating these receptors, we recorded spontaneous spiking activity extracellularly in acute brain slices of the CeA (21). Bath application of the highly specific oxytocin receptor agonist [Thr^4,Gly^7]-oxytocin (TGOT, 0.2 μM, for 30 s) (fig. S2)

(21) increased spontaneous spike frequencies in 21% of 224 recorded neurons (to 284 ± 26% of the initial frequency) but decreased them in more than 50% (to 19 ± 2%). Both responses were fully reversible and repeatable (fig. S1) and could be blocked by the oxytocin receptor antagonist d(CH$_2$)$_5$[Tyr(Me)^2,Thr^4,Orn^8,des-Gly-NH$_2$^{9}]-vasotocin (OTA, 1 μM) [TGOT excitation: 301 ± 16%, $P < 0.05$, and OTA+TGOT: 93 ± 7%, $P > 0.05$, $n = 6$ experiments (21); TGOT inhibition: 6 ± 6%, $P < 0.05$, and OTA+TGOT: 110 ± 24%, $P > 0.05$, $n = 5$ experiments; all relative values are expressed as percentages of the control frequency] (Fig. 1, B to D). Subsequent exposure of TGOT-excited cells to the general vasopressin receptor agonist [Arg^8]-vasopressin (AVP, 0.02 to 0.2 μM, for 30 s) was only able to induce small increases in frequency (Fig. 1B), which were probably caused by a cross-reactivity of AVP on oxytocin receptors (fig. S2) (21). On the other hand, AVP potently excited more than 50% of TGOT-inhibited neurons (319 ± 9%, 24 out of 47 cells) (Fig. 1, C and D). This latter effect was fully reversible and repeatable (fig. S1) and appeared mediated by V1a receptors: It could be blocked by the V1 receptor antagonist d(CH$_2$)$_5$[Tyr(Me)^2,Arg^8]-vasopressin (TMA, 1 μM) (Fig. 1D) and could be mimicked neither by the V1b receptor agonist [1-deamino-4-cyclohexylalanine]-Arg-vasopressin (d[Cha]AVP, 1 μM) (Fig. 1D) nor by the V2 receptor agonist [deamino-Cys^1,Val^4,D-Arg^8]-vasopressin (dVDAVP,

1 μM) (fig. S3). This was further confirmed by an additional combination of different vasopressin receptor agonists and antagonists (fig. S3). Thus, our findings suggest two groups of TGOT-responsive neurons in the CeA: one that is excited by oxytocin receptor activation and a second that is inhibited by activation of oxytocin receptors but excited by vasopressin V1a receptors.

Earlier morphological studies have shown intense γ-aminobutyric acid (GABA)–positive staining in the CeA and projections from the CeL/C onto the CeM, which are thought to be GABAergic (8, 22). Hypothesizing that these could mediate the inhibitory effects of oxytocin receptor activation, we determined the precise position and projections of TGOT and AVP-excited cells using sharp-electrode intracellular current-clamp recordings. Neurons were held near the spiking threshold (–55 ± 4 mV), and excitation was measured as a rapid increase in spontaneous spike frequency accompanied by small depolarizations (3.4 ± 0.4 mV and 4.6 ± 0.8 mV, respectively; $n = 6$ experiments) that were resistant to tetrodotoxin (TTX, 1 μM) (Fig. 2A). Cells with
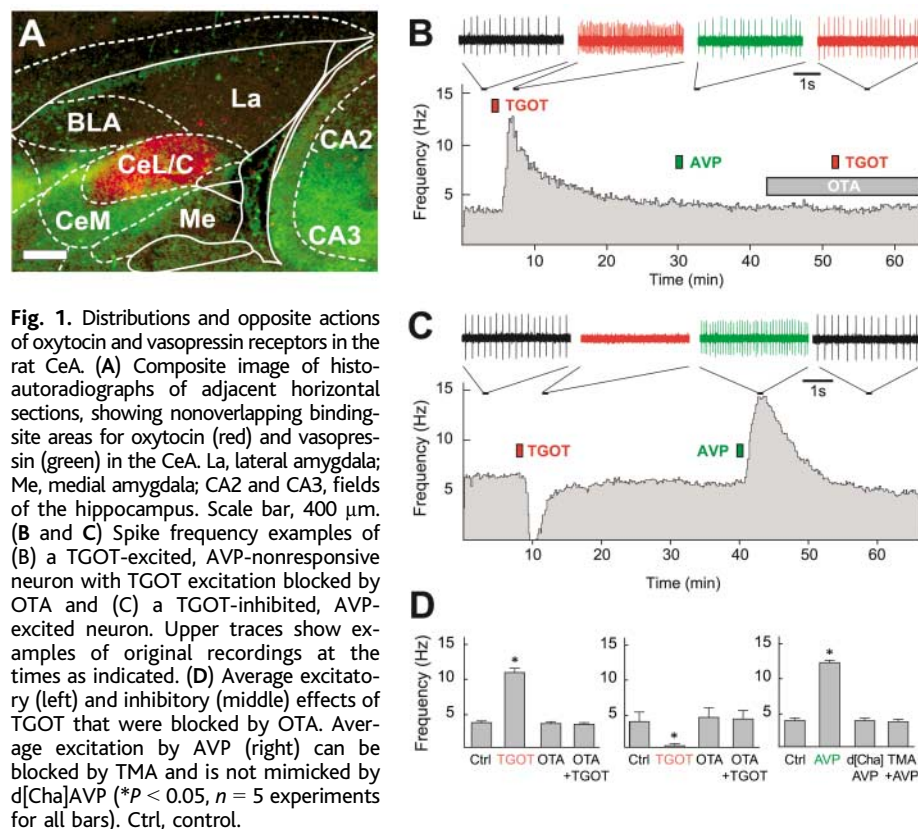

Fig. 1. Distributions and opposite actions of oxytocin and vasopressin receptors in the rat CeA. (A) Composite image of histo-autoradiographs of adjacent horizontal sections, showing nonoverlapping binding-site areas for oxytocin (red) and vasopressin (green) in the CeA. La, lateral amygdala; Me, medial amygdala; CA2 and CA3, fields of the hippocampus. Scale bar, 400 μm. (B and C) Spike frequency examples of (B) a TGOT-excited, AVP-nonresponsive neuron with TGOT excitation blocked by OTA and (C) a TGOT-inhibited, AVP-excited neuron. Upper traces show examples of original recordings at the times as indicated. (D) Average excitatory (left) and inhibitory (middle) effects of TGOT that were blocked by OTA. Average excitation by AVP (right) can be blocked by TMA and is not mimicked by d[Cha]AVP (*$P < 0.05$, $n = 5$ experiments for all bars). Ctrl, control.
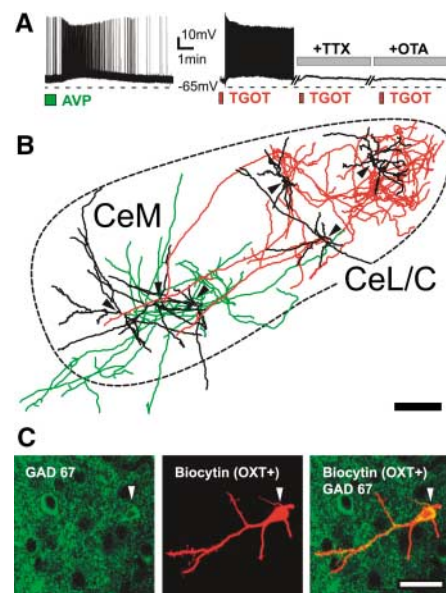

Fig. 2. Intracellular recordings and morphological properties of vasopressin and oxytocin excited neurons in the CeA. (A) Intracellular recordings of an AVP-excited neuron in the CeM (left) and a TGOT-excited neuron in the CeL/C (right) with depolarization that persisted in the presence of TTX but was blocked by OTA. (B) Morphology and projections of three oxytocin-excited (red axon collaterals) and three vasopressin-excited neurons (green axon collaterals), as revealed by biocytin injections after intracellular recordings (dendrites in black and somata marked by black arrows). Scale bar, 200 μm. (C) Neurochemical characterization of an oxytocin-excited neuron (OXT+, white arrow indicates soma) costained for GAD-67 (green) after biocytin injection (red) reveals costaining (yellow). Scale bar, 25 μm.

excitatory responses were injected with biocytin from the intracellular recording pipette ($n = 10$ experiments). AVP-excited cells were restricted to the CeM and displayed moderately spiny dendrites and medium-sized cell bodies, with axon collaterals that projected in an anteromedial direction outside the CeA. TGOT-excited neurons were found in the CeL, were of the medium-sized spiny type, and contained several local axon collaterals, of which one or more typically projected toward the CeM (Fig. 2B). Confocal microscopy revealed these TGOT-excited cells to be immunopositive for GAD-67 (Fig. 2C), confirming that they were GABAergic.

Would TGOT indeed affect GABAergic transmission in the CeM? We recorded post-synaptic currents in the CeM by the whole-cell voltage-clamp technique. Bath-applied TGOT evoked rapid increases in these currents that were blocked by OTA and completely disappeared in the presence of the GABA(A) receptor antagonist bicuculline (BIC, 20 μM) (Fig. 3A). Amplitudes and rise and decay times were not affected by 0.2 μM nor by 1 μM TGOT (Fig. 3B and table S1). Thus, TGOT appears to specifically enhance GABAergic transmission in the CeM through a rapid and reversible increase of the frequency of the inhibitory postsynaptic currents (IPSCs). Previous studies have shown that oxytocin is able to modulate synaptic transmission by a number of pre- and postsynaptic mechanisms (18). We therefore applied TGOT in the presence of TTX (1 μM) to cells that had previously responded to TGOT, but we found no significant effects on the miniature IPSC frequencies, amplitudes (Fig. 3, A and B), rise times, or decay times (table S1), which seems to exclude a postsynaptic effect by TGOT. A presynaptically mediated increase in IPSC frequency could result from an enhanced excitability of the cell body or from an increased release probability from the presynaptic site. We thus focally applied TGOT (1 μM) from a 1-μm patch pipette at the presynaptic site near the recorded neuron in the CeM, but this never caused a change in IPSC frequency (Fig. 3C, position A) ($n = 5$ experiments). Puffing of TGOT laterally, however, at distant sites in the CeL/C, was able to induce sharp increases in IPSC frequencies at specifically identified locations (Fig. 3C, position B, and table S1) ($n = 5$ experiments), which were blocked by

Fig. 3. Local effects of oxytocin on IPSCs in the CeA. (**A**) Examples of IPSC appearances in the presence of various treatments as indicated. (**B**) Average TGOT effects on IPSC frequency and amplitude in the absence and presence of TTX (left, $n = 9$ experiments); TGOT significantly enhanced mean IPSC frequency (*, $P < 0.01$) but did not affect amplitudes of IPSC or miniature IPSCs ($P > 0.1$, $n = 5$ experiments, middle and right) (table S1). Rel. Frequency, relative cumulative frequency. (**C**) Effects of local application of TGOT (1 μM) with a patch pipette in the CeM (position A) and in the CeL/C (position B) on IPSC frequency before and after TTX. R indicates the recording electrode.
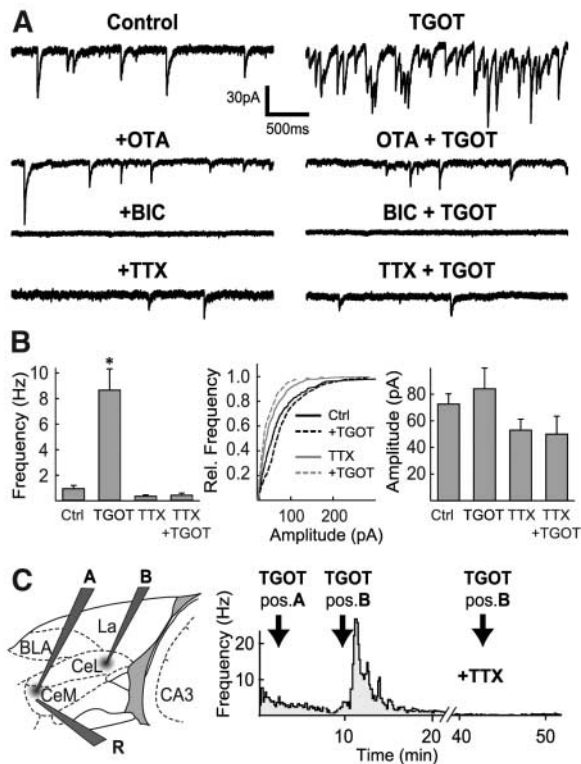

Fig. 4. Effects of oxytocin and vasopressin on the gating of inputs from different afferent pathways in the CeA. (**A**) Simplified model of local circuitry in the CeA, showing processing of different excitatory inputs (+) and GABAergic connections (–) between oxytocin and vasopressin receptor–expressing regions (CeL/C and CeM), stimulation electrode (S), and recording electrode (R). (**B**) Paired stimuli (S1 and S2, 50-ms separation, at 10-s intervals) applied to cortical afferents in the external capsule (6) resulted in excitatory potentials in CeL/C neurons under current-clamp. Stimuli were paired with postsynaptic current injections (D) such that the second stimulus (S2) regularly evoked action potentials. TGOT application (1 μM, for 1 min) caused a small depolarization of the membrane potential and increased probability of action potential generation after D, S1, or S2. The traces show superpositions of 15 sweeps, which were averaged per experiment in order to calculate the percentages of spikes evoked by each stimulus as indicated by the bar charts below (*, $P < 0.05$, $n = 5$ experiments). (**C**) Neurons in the CeM were stimulated through their afferents in the basolateral and basomedial nuclei (22). AVP (0.2 μM, for 1 min) caused similar effects as TGOT in the CeL, whereas subsequent administration of TGOT (1 μM, for 1 min) led instead to decreases in responses to S1 and S2 (*, $P < 0.05$, $n = 5$ experiments).
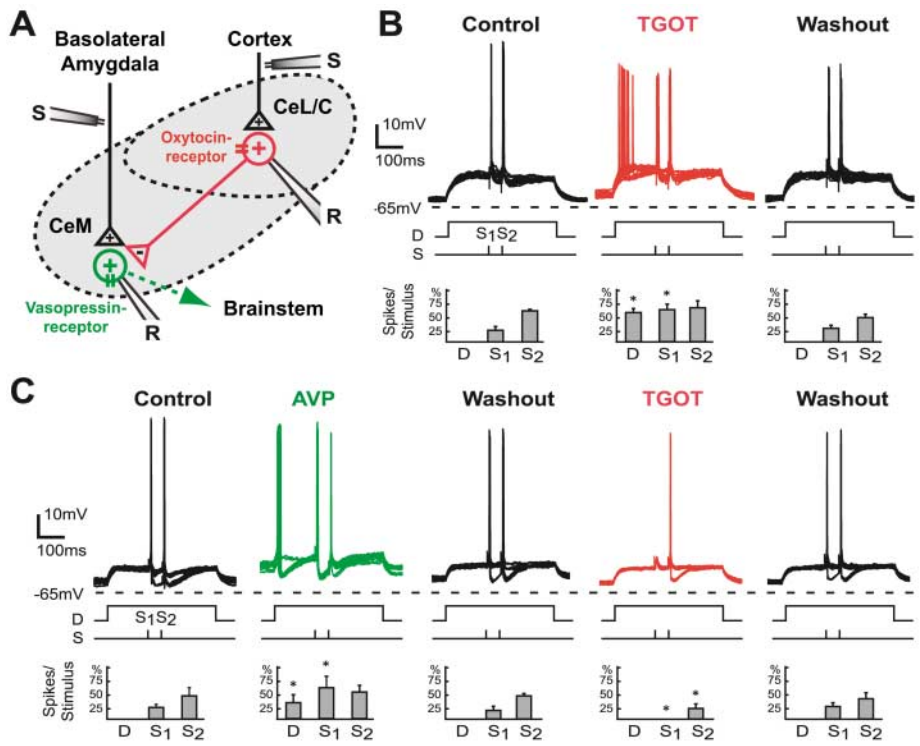
subsequent application of TTX. These findings indicate that the inhibitory effects of TGOT are caused by an enhanced excitability of neurons in the CeL/C that leads to an increase of GABA release in the CeM.

Changes in the excitability of neurons in different subnuclei may be relevant to the behavioral function of the CeA, because they can modulate the integration of its distinct inputs (1). The CeL/C receives projections from cortical and subcortical areas (6, 8) and projects to the CeM, which also receives direct input from the basolateral amygdala (BLA) (Fig. 4A) (22). We indeed found that during stimulation of the excitatory afferents to the CeL/C, TGOT could enhance the probability of evoking postsynaptic action potentials (Fig. 4B). During stimulation of the excitatory afferents to the CeM, however, TGOT decreased the probability of evoking postsynaptic action potentials, but AVP increased it (Fig. 4C).

These findings reveal two major points. First, vasopressin and oxytocin modulate activity in CeM neurons in opposite ways through the activation of distinct elements of an inhibitory network (Fig. 4A). Second, through the activation of these distinct elements, vasopressin and oxytocin can differently affect the integration of distinct afferents to the CeA into a common output to the autonomic nervous system, thus providing a neurophysiological mechanism for their opposite effects on anxiety and fear behavior. As we have previously found a comparable distribution of oxytocin and vasopressin receptors throughout the central extended amygdala (9), this mechanism may also apply to regions that include the bed nucleus of the stria terminalis and parts of the nucleus accumbens. These latter structures are known to be involved in the control of anxiety, stress, motivation, and addiction (23) and are possibly regulated by vasopressin and oxytocin in a similar manner.

The results of this study suggest that the endogenous balance between oxytocin and vasopressin receptor expression and activation may set distinct, individually tuned levels for the activation of the autonomic fear response. The levels of these neuropeptides in the extracellular fluid of the CeA are increased during stress (12, 24), possibly through release from local vasopressinergic and oxytocinergic fibers (25, 26). Furthermore, variations in levels of receptor expression and injections of specific antagonists have been directly correlated with changes in anxiety and fear (12, 16, 17, 24, 27, 28). Together, these findings confirm the physiological and behavioral relevance of the proposed mechanism. Anxiety and fear can directly affect parental care, thereby modulating the expression of oxytocin and vasopressin receptors in offspring and establishing anxiety and fear traits that can be

carried over several generations (16, 27). The elucidation of the opposite, modulatory mechanism of these two peptides in the CeA provides a solid rationale for the development of new, individually tailored treatments, working in concert with the more traditional GABAergic agonists (4, 5). Indeed, the vasopressin receptor could be a pharmacological target for the treatment of stress and anxiety-related disorders (10, 11).

Several recent lines of evidence suggest that fear extinction inhibits the expression of the conditioned reaction rather than erasing the memory (3). This inhibition is thought to be mediated by cortical afferents to the amygdala, originating in the medial prefrontal cortex (7). Our findings provide evidence for a functional link between cortical input in the CeL/C and inhibition of output from the CeA. The oxytocinergic modulation of the cortical input and the vasopressinergic effects on input from the BLA could implicate additional, opposing roles for these neuropeptides in fear extinction.

References and Notes

1. J. E. LeDoux, *Annu. Rev. Neurosci.* **23**, 155 (2000).
2. P. Sah, E. S. Faber, M. Lopez De Armentia, J. Power, *Physiol. Rev.* **83**, 803 (2003).
3. D. Pare, G. J. Quirk, J. E. Ledoux, *J. Neurophysiol.* **92**, 1 (2004).
4. Z. Nie *et al.*, *Science* **303**, 1512 (2004).
5. M. H. Kang-Park, W. A. Wilson, S. D. Moore, *Neuropharmacology* **46**, 1 (2004).
6. A. J. McDonald, S. J. Shammah-Lagnado, C. Shi, M. Davis, *Ann. N.Y. Acad. Sci.* **877**, 309 (1999).
7. G. J. Quirk, E. Likhtik, J. G. Pelletier, D. Pare, *J. Neurosci.* **23**, 8800 (2003).
8. M. D. Cassell, L. J. Freedman, C. Shi, *Ann. N.Y. Acad. Sci.* **877**, 217 (1999).
9. P. Veinante, M. J. Freund-Mercier, *J. Comp. Neurol.* **383**, 305 (1997).
10. G. Griebel *et al.*, *Proc. Natl. Acad. Sci. U.S.A.* **99**, 6370 (2002).
11. I. F. Bielsky, S. B. Hu, K. L. Szegda, H. Westphal, L. J. Young, *Neuropsychopharmacology* **29**, 483 (2004).
12. R. Landgraf, I. D. Neumann, *Front. Neuroendocrinol.* **25**, 150 (2004).
13. G. L. Kovacs, D. deWied, *Pharmacol. Rev.* **46**, 269 (1994).
14. R. J. Windle, N. Shanks, S. L. Lightman, C. D. Ingram, *Endocrinology* **138**, 2829 (1997).
15. J. N. Ferguson *et al.*, *Nature Genet.* **25**, 284 (2000).
16. F. Champagne, J. Diorio, S. Sharma, M. J. Meaney, *Proc. Natl. Acad. Sci. U.S.A.* **98**, 12736 (2001).
17. T. L. Bale, A. M. Davis, A. P. Auger, D. M. Dorsa, M. M. McCarthy, *J. Neurosci.* **21**, 2546 (2001).
18. M. Raggenbass, *Prog. Neurobiol.* **64**, 307 (2001).
19. Y. F. Lu *et al.*, *Brain Res.* **768**, 266 (1997).
20. M. Condes-Lara, P. Veinante, M. Rabai, M. J. Freund-Mercier, *Brain Res.* **637**, 277 (1994).
21. Materials and methods are available as supporting material on *Science* Online.
22. V. Savander, D. G. Go, J. E. Ledoux, A. Pitkanen, *J. Comp. Neurol.* **374**, 291 (1996).
23. G. F. Koob, *Eur. Neuropsychopharmacol.* **13**, 442 (2003).
24. K. Ebner, O. Bosch, S. A. Kromer, N. Singewald, I. D. Neumann, *Neuropsychopharmacology* **30**, 223 (2005).
25. M. W. Sofroniew, *Trends Neurosci.* **6**, 467 (1983).
26. G. J. de Vries, R. M. Buijs, *Brain Res.* **273**, 307 (1983).
27. D. D. Francis, L. J. Young, M. J. Meaney, T. R. Insel, *J. Neuroendocrinol.* **14**, 349 (2002).
28. D. A. Lubin, J. C. Elliott, M. C. Black, J. M. Johns, *Behav. Neurosci.* **117**, 195 (2003).
29. We thank M. Raggenbass for introducing us to the exciting world of neuropeptides and F. Magara, E. Welker, M.-C. Broillet, and P. Magistretti for critical reading and comments to the manuscript. Supported by grants from the Swiss National Science Foundation, the Roche Research Foundation, and the Novartis and Théodore Ott Foundations.

Dependence of Self-Tolerance on TRAF6-Directed Development of Thymic Stroma

Taishin Akiyama,[1] Shiori Maeda,[1] Sayaka Yamane,[1] Kaori Ogino,[1] Michiyuki Kasai,[2] Fumiko Kajiura,[3] Mitsuru Matsumoto,[3] Jun-ichiro Inoue[1]*

The microenvironments of the thymus are generated by thymic epithelial cells (TECs) and are essential for inducing immune self-tolerance or developing T cells. However, the molecular mechanisms that underlie the differentiation of TECs and thymic compartmentalization are not fully understood. Here we show that deficiency in the tumor necrosis factor receptor–associated factor (TRAF) 6 results in disorganized distribution of medullary TECs (mTECs) and the absence of mature mTECs. Engraftment of thymic stroma of *TRAF6*−/− embryos into athymic nude mice induced autoimmunity. Thus, TRAF6 directs the development of thymic stroma and represents a critical point of regulation for self-tolerance and autoimmunity.

Thymic epithelial cells (TECs) establish spatially distinct microenvironments that are essential for generating a T cell repertoire.

Cortical TECs (cTECs) are involved in selecting thymocytes that are capable of recognizing self–major histocompatibility complex (1),